INTERNATIONAL JOURNAL OF INTEGRATED ENGINEERING
ISSN: 2229-838X e-ISSN: 2600-7916

IJIE

Vol. 16 No. 5 (2024) 311-323
https://publisher.uthm.edu.my/ojs/index.php/ijie

Mutual Coupling Reduction of Super Wide Band MIMO Antenna Using Metamaterial Periodic Defected Ground Structures for THz Applications

Ranjana Kumari[1,2], V.K. Tomar[1]*

[1] *Department of Electronics and Communication Engineering, GLA University, Mathura, Uttar Pradesh, INDIA*
[2] *Department of Electronics and Communication Engineering, Galgotias College of Engineering and Technology(GCET), Greater Noida, Uttar Pradesh, INDIA*

*Corresponding Author: vinay.tomar@gla.ac.in
DOI: https://doi.org/10.30880/ijie.2024.16.05.024

Article Info

Received: 20 January 2024
Accepted: 18 May 2024
Available online: 12 August 2024

Keywords

Super wide-band MIMO antenna (SWBMA), double negative meta-material DNG-PDGS, S-parameters, envelope correlation coefficient (ECC), TARC (dB), CCL (bps/Hz)

Abstract

In this article, a double negative (DNG) material inspired periodic defected ground structure is presented to reduce mutual coupling and gain enhancement of super wide band multiple input and multiple output antenna (SWBMA) for terahertz (THz) applications. For THz applications, a dual port super wide band MIMO antenna with size of 0.35 λ_0 ×0.17 λ_0 ×0.02 λ_0 (57 ×27.6 ×3.36 μm^3) has been designed on quartz substrate. The simulated results of proposed antenna exhibit fractional bandwidth (FWB) of 164% at 9.9THz resonant frequency (1.75 to 18THz) with peak gain 9.2dBi, and average radiation efficiency 89% throughout the super wide band spectrum. By inserting DNG meta-material based periodic defected ground structures in between inverse L stubs on ground plane, an isolation S_{12}/S_{21} between radiating elements of $S_{i,j} \leq$ -25dB has been attained. MIMO parameters of designed antenna are also investigated and it is observed that ECC<0.0025, DG>9.98 dB, TARC<-15dB, MEG<-3dB, and CCL<0.225bps/Hz throughout spectrum of antenna.By evaluating the characteristics of proposed antenna, it can be concluded that the proposed MIMO antenna can be a good candidate for high-speed THz applications like future 6G, high-speed Radar, and radiometric applications.

1. Introduction

THz communications have gained considerable attention for providing a communication link with high speed and increased channel capacity in [1]. Due to the high penetration power feature, THz radiation can also be utilized for material characterization in [2]. To utilize these features of the THz regime, the design of compact antennas with effective gain and radiation efficiency has attracted a lot of attention from researchers in [3]-[4]. But these antennas face high complexity which increases the difficulty in the design process of antennas. Thus, to reduce the complexity, metamaterial and layered-based antennas have been introduced in [5]-[6]. However, the use of layered-based antennas increases their profile. Further, because of single-element utilization in [2]-[6], the system faces multipath fading problems, and the system degrades performance in terms of signal errors in communication links. Multipath fading can be minimized by the utilization of diversity techniques in multiple input multiple outputs (MIMO) links like spatial diversity, pattern diversity, and polarization diversity presentations. Recently, a lot of research has been done on different diversity practices to improve diversity features of the MIMO structure which depend on decoupling structure utilization at front & back side of substrate.

Few authors have investigated numerous techniques for suppressing the effect of mutual coupling among radiating elements. In [7], Split ring resonators (SRR)with inductive and capacitive effect has been designed in the form of decoupling structure. To achieve isolation in broadband, multi-resonant stubs have been formed in tree shape decoupling structures on ground plane [8]. Other decoupling structures like etching defected ground structure (DGS) in [9], slotted type defected ground structure (DGS) [10], slots on the ground [11], and fractal-based DGS structure in [12] have been designed to reduce mutual coupling effect. Another approach is the electromagnetic band gap (EBG) structure which behaves as a stop band filter and does not allow wave propagation in a specific frequency spectrum [13]. EBG and SRR are employed between radiating elements to enhance isolation parameters [14]. Metamaterial unit cells, featuring decoupling networks, are designed to improve isolation in monopole antennas [15]. For MIMO antennas, a complementary split ring resonator (CSRR) with a neutralizing line is utilized to suppress mutual effects [16]-[17]. Additionally, a modified serpentine structure with band-filter characteristics is employed to mitigate mutual coupling effects [18].

Further, two-element THz MIMO antennas are proposed in [19]-[23] for acquiring high data rate as well as channel capacity. In [19], a MIMO antenna with parallel arrangement of radiating elements is investigated, demonstrating an impressive isolation level exceeding -23dB, and volume of antenna configuration is 820×1000×81.29 µm3.To achieve ultra-wideband, a tetradecagonal ring-shaped has been utilized to design two antennas structure with sizes 800×1220µm2 and 800×1170 µm2. Also compared with spatial and pattern diversity techniques to determine the isolation S21<-20dB for wider impedance bandwidth in [20]. For high-speed THz applications, two port elliptical shape patch MIMO antenna with spatial diversity is printed on 1000×1400×101.29 µm3 substrate in [21] having high isolation between radiating elements due to effect of inverting L stubs at ground plane with minimum radiating efficiency 70% at lower frequency spectrum. In [22], a compact MIMO antenna is designed at operating frequency 8.2THz with peak gain 8.2 dB and -22dB minimum isolation. Moreover, the analysis of specific absorption rate (SAR in W/Kg) has also been simulated at different input powers for WBAN application. In [23] graphene-based tree shaped MIMO antenna is presented with physical size of 600×300 µm2, offers narrow impedance bandwidth (88.14%) with peak gain (4dBi) and, low mutual coupling (S21<-20dB) between radiating element. In [24], a MIMO antenna has been designed with mushroom metamaterial structure, offers zero order characteristics at frequency 3THz which reduce the isolation less than -22.1 dB in intended spectrum.

As per observation from [19],[20],[21],[23], and [24], MIMO antennas have several advantages but few of them having high profile with high level isolation and most of antenna have employed defected ground structures. Nevertheless, the presence of a defected ground structure (DGS) has a notable impact on the stability of the radiation characteristics and the overall efficiency of the antenna. This effect arises from the leakage of signals occurring from the rear side of the antenna across the entire frequency spectrum. In [24], because of vertical placement of meta-surface between antenna, the overall profile of antenna increases.

Therefore, in this article, DNG (double negative) metamaterial based periodic defected ground structures have been implanted in between inverse L stubs on the ground plane for low mutual coupling and gain enhancement throughout the frequency spectrum. The physical footprint of proposed antenna with 0.35 λ0×0.17 λ0 ×.02 λ0 µm3 exhibits a super wideband (SWB) with impedance bandwidth 1.75 to 18THz (164%). According to simulated S-parameters, DNG-based periodic defected ground structures have been inserted in between inverse L stubs at the ground which improves the isolation(S12/S21) as well as diversity performance in terms of envelope correlation coefficients (ECC), diversity gain (DG), total active reflection coefficient (TARC), and channel capacity(bps/Hz).

The research article is ordered as follows: methodology of proposed dual-port MIMO antenna with & without DNG based periodic defected ground structure has been discussed in section II.Results & discussions, diversity parameters analysis, and comparison between the proposed antenna and previously reported antennas are presented in section III.In concluding section, section V, the research article provides a summary and final remarks on the findings and implications of the study.

2. DNG-Periodic Defected Ground Structure (DNG-PDGS) Loaded Dual Port MIMO Antenna Methodology

2.1 Progression of Opposite Connected C(O-CC) DNG Loaded Single Element Antenna

To acquire the super wide band, the progression of the single antenna is accomplished in five steps (Ant.1-Ant.5) as presented in Fig. 1(a)-Fig. 1(g). The physical dimensions of Ant.1-Ant.5 are discussed in table 1. Quartz substrate has been utilized with a thickness of 3.36µm, dielectric constant Ɛr=3.75, and tangent loss 0.0001 in Ant1- Ant.5.To verify the effectiveness of super wideband spectrum, each stage of antenna (Ant.1-Ant.5) is designed and simulated by CST Microwave Studio 2019. In Fig. 1(a), a simple square patch with physical dimensions of 9.8 x 9.8 µm2 (Lp x Lp) is connected by a microstrip feed line with dimensions Wf1=2.76 µm and Lf1=10µm in Ant.1. Ant.1 is implanted on a quartz substrate with dimensions of 28 x 27x3.36 µm3 (Ls x Ws x t).

Int. Journal of Integrated Engineering Vol. 16 No. 5 (2024) p. 311-323

On the back side of substrate, a partial ground with 27.6 x 8.6 µm2 dimensions is implanted for acquiring the wideband spectrum. The reflection coefficients/S11 of Ant. 1 is described in Fig. 2. As per observation, Ant.1 offers (S11≤-10 dB) impedance bandwidth at 9.7 to 18 THz with 60% fractional bandwidth (FBW). To increase fractional bandwidth (%), the geometry of a square patch with partial ground is altered from Ant.1-Ant.5 which are shown in Fig. 1(a)-(g). The impact of modifications on S11 parameters is illustrated in Fig. 2.

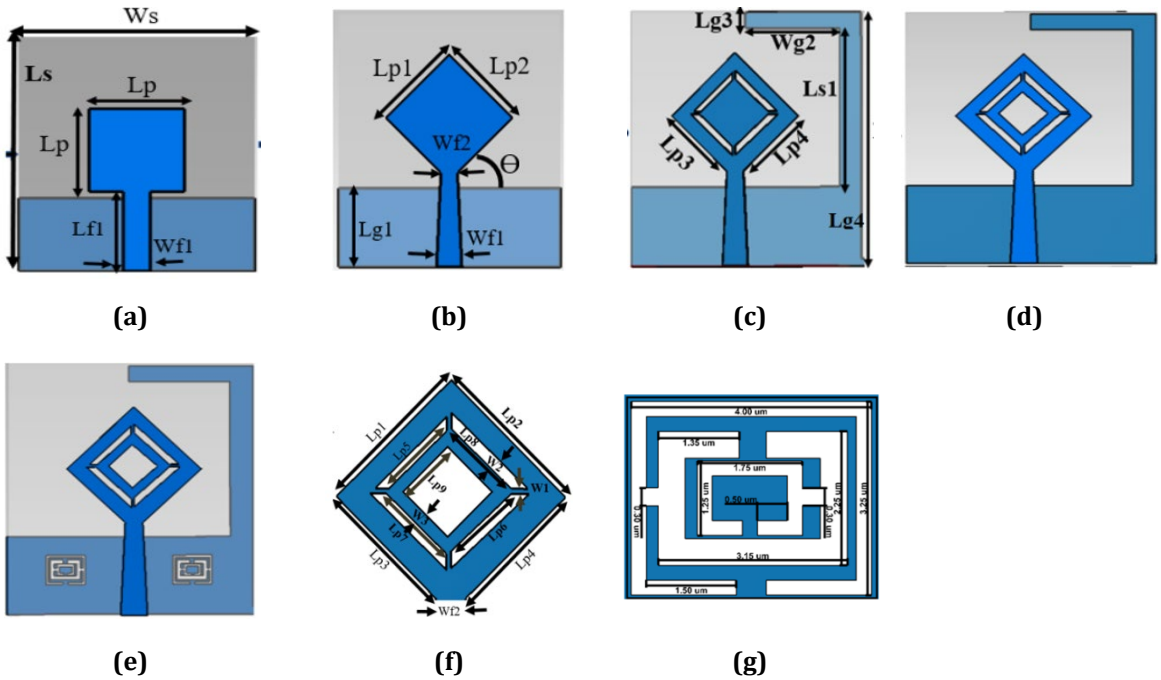

Fig. 1 *Progression of single element antenna (a) Ant.1; (b) Ant.2; (c) Ant 3; (d) Ant.4; (e) Ant.5; (f) Enlarge view of radiating element of Ant.5; (g) DNG O-CC unit cell with dimensions*

Further, to enhance the bandwidth at the lower frequency side, a rhombus shape patch with dimensions Lp1=Lp2 and Lp3=Lp4 has been designed by rotating square-patch with 450 and it is connected by a tapered feed with dimensions of Wf1=2.71 µm, Wf2=1.8 µm in Ant. 2. As per observation in Fig. 2, the improved impedance bandwidth of Ant.2. is 138% fractional bandwidth at 3.3THz to 18THz. To attain fractional bandwidth of 164%, four slots with physical lengths Lp5, Lp6, Lp7, and Lp8 with same slots width w2 are etched out from a rhombus shape patch, and one more inverse L shape stub with the size of 19x10.37 µm2(Ls1xWg2) and width Lg3=1.73µm is connected at the ground in Ant.3.

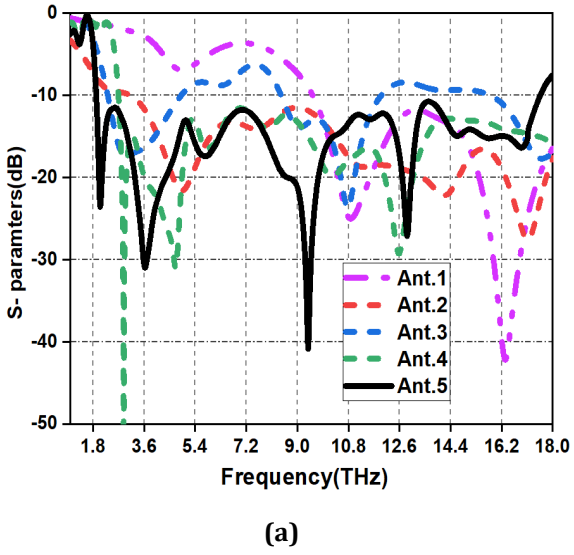

Fig. 2 *Simulated results (a) progression of single antenna*

These modifications alter the current path in long path which produces the additional resonance in the frequency spectrum as illustrated in Fig. 2. As per discussion, return loss/S11 of Ant.3 has shifted to a lower frequency at 2.12THz. However, impedance matching is not good enough in frequency ranges from 5.13 THz to 8.2 THz and 11.2 THz to 15.8 THz respectively.

Therefore, to provide good impedance matching at the lower frequency, one more slot with Lp9xLp9 um^2 is etched out from radiating element in Ant.4 which also provides the longer current path to the proposed antenna which assistance to improve impedance matching and bandwidth as illustrated in Fig 2. According to the simulated results, S11-parameters show impedance bandwidth of 2.7 to 18THz with fractional bandwidth (147%). Furthermore, two DNG-based O-CC metamaterial structures are placed adjacent to the feed line in Ant.5 which assists in impedance matching and bandwidth (%) enhancement as illustrated in Fig 2. After simulation of Ant.5, simulated S11 exhibited the impedance bandwidth at 1.81 to 17.5THz (162.4%) as illustrated in Fig. 2. To understand the clear physical dimensions of slots on radiating elements and DNG-O-CC metamaterial structure, the enlarged view has been illustrated in Fig. 1(f)-Fig. 1(g). All physical dimensions of proposed antenna have been discussed in Table1.To validate DNG-O-CC metamaterial structure, design of unit cell has been analyzed in next sub section.

Table 1 *Physical dimensions of proposed antenna*

Parameters	Dimension (μm)
L_SUB	27.65
W_ SUB	57
Wf1	2.76
Lf	10.1
Wf2	1.8
Θ	45^0
t	3.36
Lp1	9.78
Lp2	9.78
Lp5	4.85
Lp6	4.96
Lp7	5.02
Lp8	5.09
W1	0.5
Wg1	23
Wg2	10.37
Wg3	6.57
Lg1	8.64
Lt	3
Ls1	19
Le	19.5
Lt	3
Lg4	26.78
W2	1.5
Lp3	8.5
Lp4	8.5
Lg2	17.28
Lg3	1.73
hp	.035

2.2 Analysis of Double Negative (DNG) Metamaterial Unit Cell

According to Authors [25]-[27], negative refractive index characteristics of unit cells have been acquired when permeability, as well as permittivity of unit cells, would also be negative and DNG metamaterial enhance impedance bandwidth as well as gain of antenna. Initially, the opposite connected C shaped unit cell has been

Int. Journal of Integrated Engineering Vol. 16 No. 5 (2024) p. 311-323

designed on quartz substrate and two electromagnetic ports are applied on the positive & negative of z-axis to analyze characteristics of unit cell.

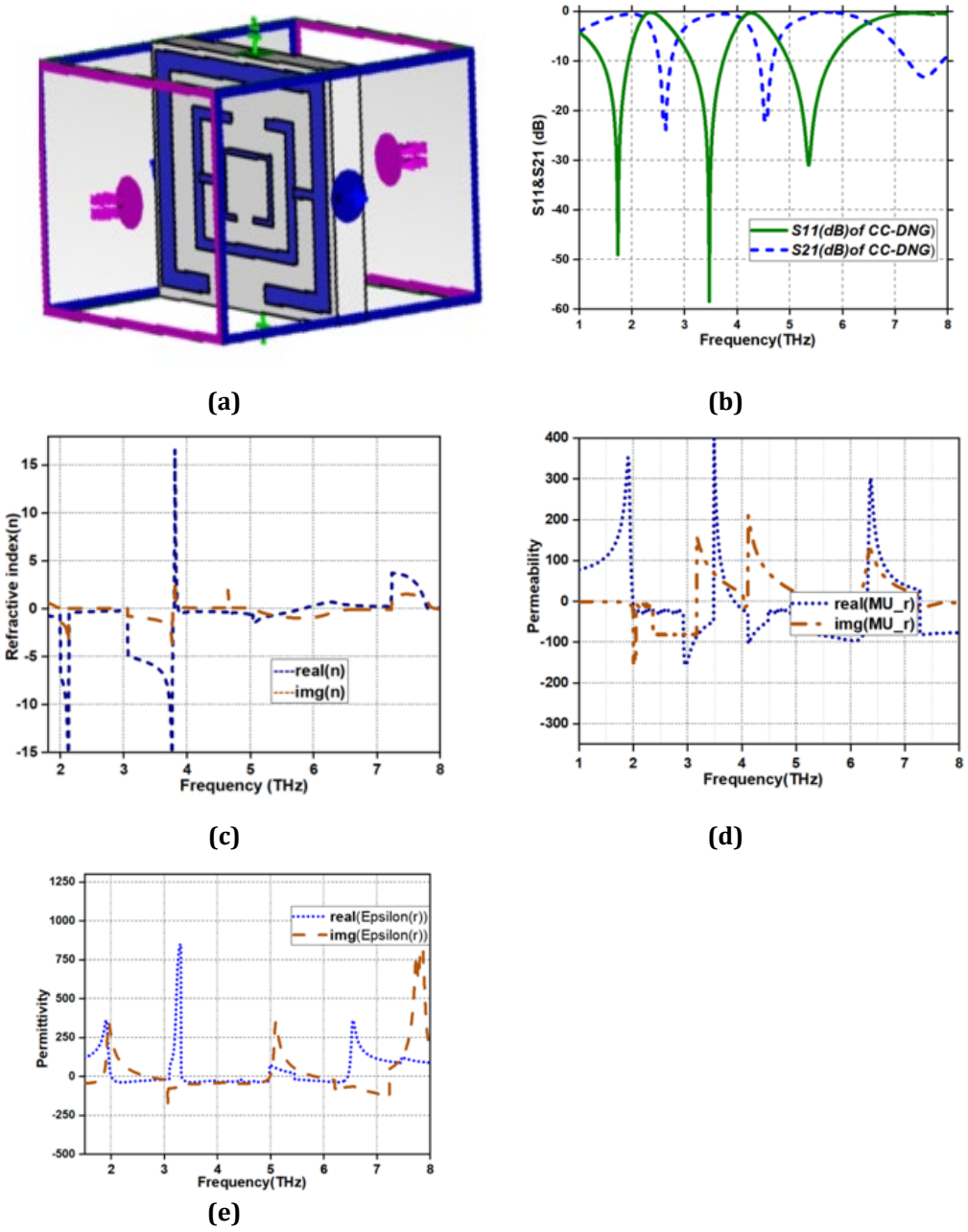

Fig. 3 *Simulated parameters of unit cell (a) Connected ports with boundary conditions; (b) Simulated S11& S21; (c) Simulated refractive index; (d)Permeability; (e) Permittivity of DNG O-CC unit cell*

The x-axis is assigned the perfect electric (PE) boundary condition, while the y-axis is assigned the perfect magnetic (PM) boundary condition as described in Fig.3(a). The simulations of S11 and S21 parameters are done in CST microwave studio 2019 which is illustrated in Fig.3(b). To validate the double negative characteristics of the unit cell, the refractive index (nr) , permeability (Ɛr), and permittivity (μr) are also computed by the Nicolon_Ross_Wier approach. Before computations of material characteristics, initially, Z1 and Z2 are calculated with magnitude of S11 and S21 respectively. Equation (1)-(2) are utilized to calculate the Z1 and Z2. After

$$S_{11} = |S_{11}|e^{i\theta_{11}} \quad (1)$$

$$S_{21} = |S_{21}|e^{i\theta_{21}} \quad (2)$$

$$Z_1 = S_{21} + S_{11} \quad (3)$$

$$Z_2 = S_{21} - S_{11} \quad (4)$$

$$\mu_r = \frac{2}{jk_0 t} \times \frac{1 - Z_2}{1 + Z_2} \quad (5)$$

$$\epsilon_r = \frac{2}{jk_0 t} \times \frac{1 - Z_1}{1 + Z_1} \quad (6)$$

$$n_r = \frac{2}{jk_0 t} \sqrt{\frac{(S_{21} - 1)^2 - {S_{11}}^2}{(S_{21} + 1)^2 - S_{11}^2}} \quad (7)$$

calculating the values of Z1 and Z2, equations (5)-(7) are utilized to compute of n_r, ε_r andμr of the unit cell of metamaterials by Nicolon_Ross_Wier approach in [28] as illustrated in Fig.3(c)-(e). Here k0 and t are the wave number and substrate thickness respectively. The computed records of n_r, ε_r andμ_r of the DNG unit cell have been discussed in Table 2. The active region for double negative metamaterial is 2.0 - 3.0THz, 3.25-3.5 THz, 4.0-6.4 THz which exhibits the double negative characteristics in O-CC unit cell.

Table 2 *Negative characteristics vs frequency spectrum of O-CC-DNG unit cell*

Characteristics	Negative THz Frequency region
permittivity_Active region	2.0 - 3.5, 4 - 6.5, 7.25 - 8
permeability_Active region	2.0 - 3.0 ,3.25 – 5.0, 5.4-6.4
refractive Index _Active region	2-2.2, 3.0 - 3.75,4.0-5.7
Double Negative Region (DNG) _Active region	2.0 - 3.0, 3.25-3.5, 4.0-6.4

2.3 DNG-Periodic Defected Ground Structure (DNG-PDGS) Loaded Dual Port MIMO Antenna

Once the structure of DNG loaded rhombus-shaped single antenna (Ant.5) is designed in Fig1(e), a single antenna (Ant.5) is transfigured into 2-port MIMO antenna to increase data rate and channel capacity(bps/Hz) as illustrated in Fig.4.Initially,the structure-I of proposed antenna is implanted on a quartz substrate with an optimized physical dimension of 57µm x 27.65µm(W_SUB X L_SUB) as illustrated in Fig.4(a).Two radiating elements are placed adjacent at a minimum distance(λ0/4) to maintain compactness of antenna in spatial diversity. Further, for the reduction of coupling effects, two inverse-L stubs with connected ground have been introduced at the ground side as illustrated in Fig.4(a). The minimum distance between antenna elements is 19.5 µm which utilized to maintain the standard value of isolation (S12/S21≤- 15dB) in the frequency region of 1.9 to 18 THz which is depicted in Fig.5a. To improve the isolation and gain, a periodic defected ground structure with DNG characteristics has been implanted at back side of substrate without altering the physical size of antenna structure I as illustrated in Fig.4(b). The top view, bottom view, and perspective view of the SWBMA with physical dimensions are depicted in Fig.4(a)-(c).

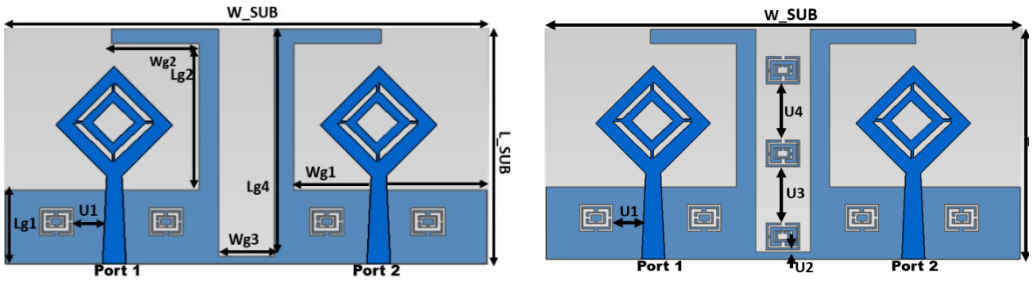

(a) **(b)**

Int. Journal of Integrated Engineering Vol. 16 No. 5 (2024) p. 311-323

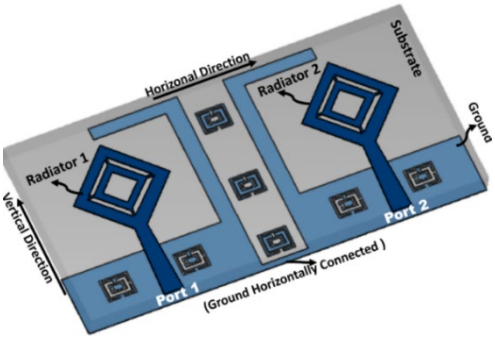

(c)

Fig. 4 *DNG loaded proposed antenna(a) Structure I;(b) Structure II; (c) Perspective view of structure II*

3. Results and Discussions

After designing, simulations of proposed antenna structures (I &II) are done by CST microwave studio 2019 software. Because of similar radiating elements, the simulated reflection coefficients (S11/S22) and transmission coefficients(S12/S21) are the same at port1& port2.

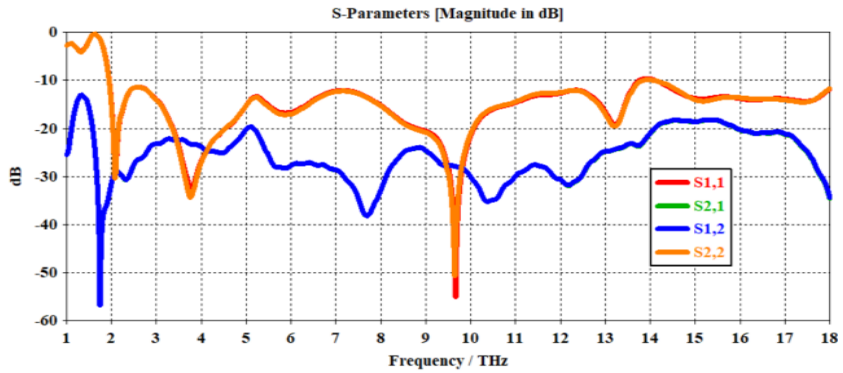

(a)

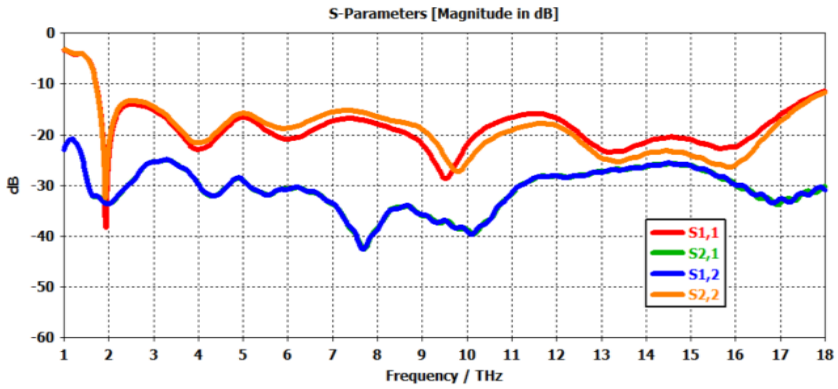

(b)

Fig. 5 *S-parameters of proposed MIMO antenna for (a) Structure I;(b) Structure II*

The reflection coefficient (S11) of the antenna expresses how much power is reflected from the antenna port1. The value of reflected power at the port should be less than -10dB. As per simulated results in Fig.5(a), the S11/S22 shows an impedance bandwidth of proposed antenna (1.9 -18THz) which also illustrates the operating frequency range of the structure I antenna. The transmission coefficient (S12) of the antenna expresses the power received at port 1 relative to the input applied power at port 2. The transmission coefficient(S12/S21) is also expressed as an isolation parameter that attains less than -15dB the standard value throughout the frequency spectrum. In Fig.5(a), due to insertion of pair of inverse L stubs at ground, S21<-18dB has been acquired in frequency range 14 to 16 THz which is not enough for MIMO wireless communication system performance in the

intended frequency spectrum(1.9-18THz). To improve isolation performance, three DNG metamaterial based periodic defected ground structures (DNG-PDGS) are loaded on ground of MIMO structure II. So, the lower frequency of proposed antenna has been shifted to 1.75 THz which increases impedance bandwidth with 164% and the transmission coefficient(S12/S21) of structure II has been improved due to effect of double negative (DNG)characteristics metamaterial as illustrated in Fig.5(b). According to simulated results, minimum value of S12 is -25dB and maximum value of isolation is -43dB for throughout super wideband(SWB)spectrum which exhibits the excellent diversity analysis of reported antenna. To validate the isolation $S_{i,j} \leq$-25dB,impact of isolation on the surface current distributions(A/m) are illustrated at different frequencies when port 1 is excited in Fig.7(a)-(d). As per observations, surface current densities at 1.89 THz, 6.5 THz, 12.5THz, and 15.5THz are concentrated at the outer edges of radiating patches as well as tapered feed line and less concentration at the bottom side of port2 which exhibits high level isolation between radiating elements.

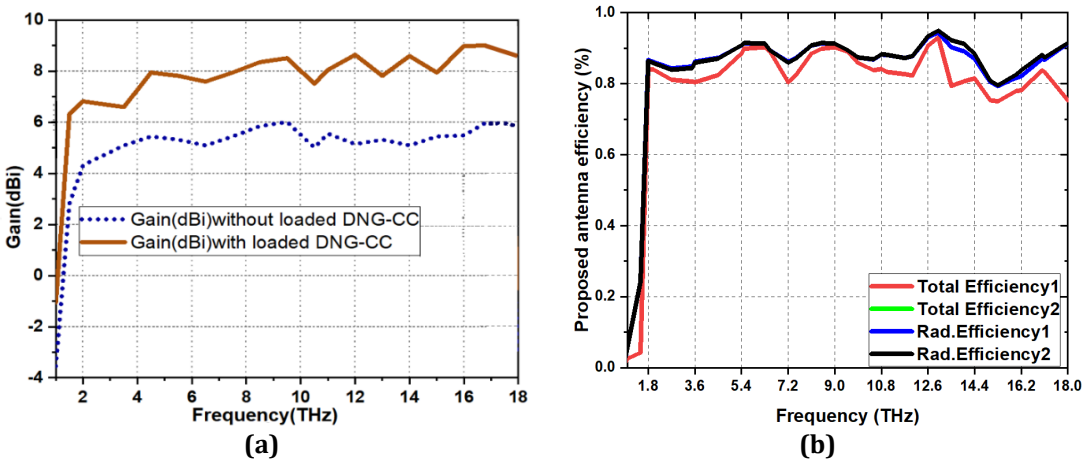

Fig. 6 *Simulated results(a) Gain(dBi) with & without loaded DNG ;(b) Efficiencies (%)*

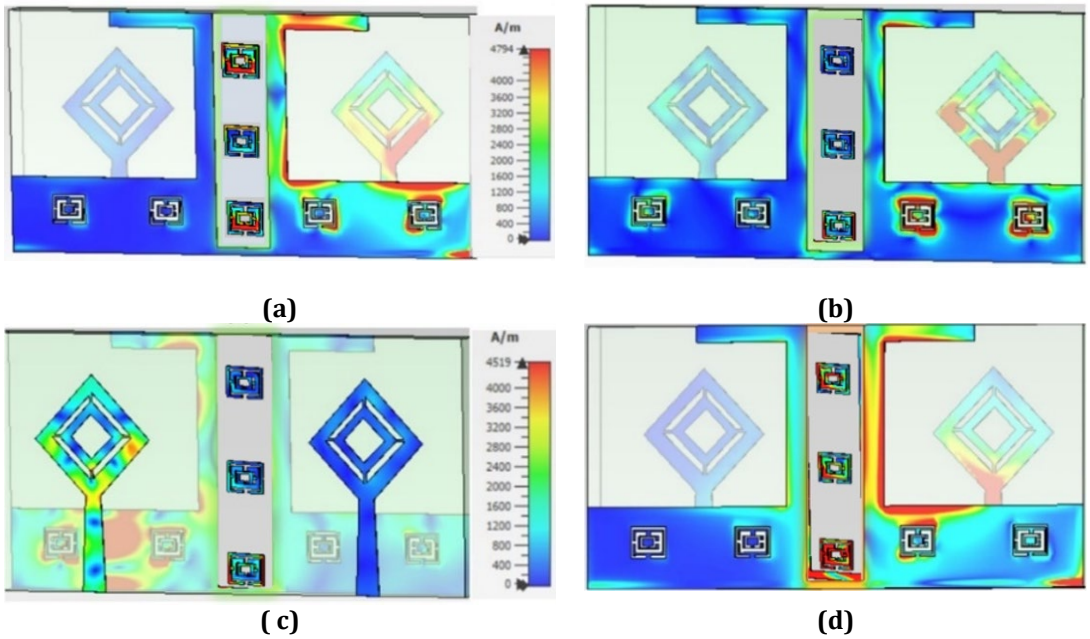

Fig. 7 *Surface current density distributions (a)1.89 THz; (b)6.5 THz ;(c)12.5THz ;(d)15.5THz*

Moreover, simulated gain and radiation efficiencies of the proposed antenna loaded with DNG material at ports 1&2 are illustrated in Fig.6(a)-(b). As per observation, the gain of DNG-PDGS loaded structure is progressively increasing and gain is constant from 3.6 to 15.3THz. In Fig.6(a), the maximum gain of 9.2 dBi is observed which is high as compared to structure-I at upper-frequency 18 THz. According to the illustration in Fig.6(b), the average values of total efficiency and radiation efficiency are almost 87% and 89% respectively which also exhibits good performance of proposed antenna. Moreover, the radiation characteristics of the designed antenna in the XZ-plane (H plane) and YZ-plane (E plane) have been analyzed at 2THz,5THz, and 15THz frequencies and described in Fig.8(a)-Fig.8(f). It is observed that stable radiation patterns are quasi-

Int. Journal of Integrated Engineering Vol. 16 No. 5 (2024) p. 311-323

omnidirectional and complementary in E plane (YZ plane) & H plane (XZ plane), the complementary radiation in nature acquires minimum mutual coupling as well as correlation between radiators. The cross-polarization is less than -20 dB in maximum radiation field direction as illustrated in Fig.8(a)- Fig.8(f).

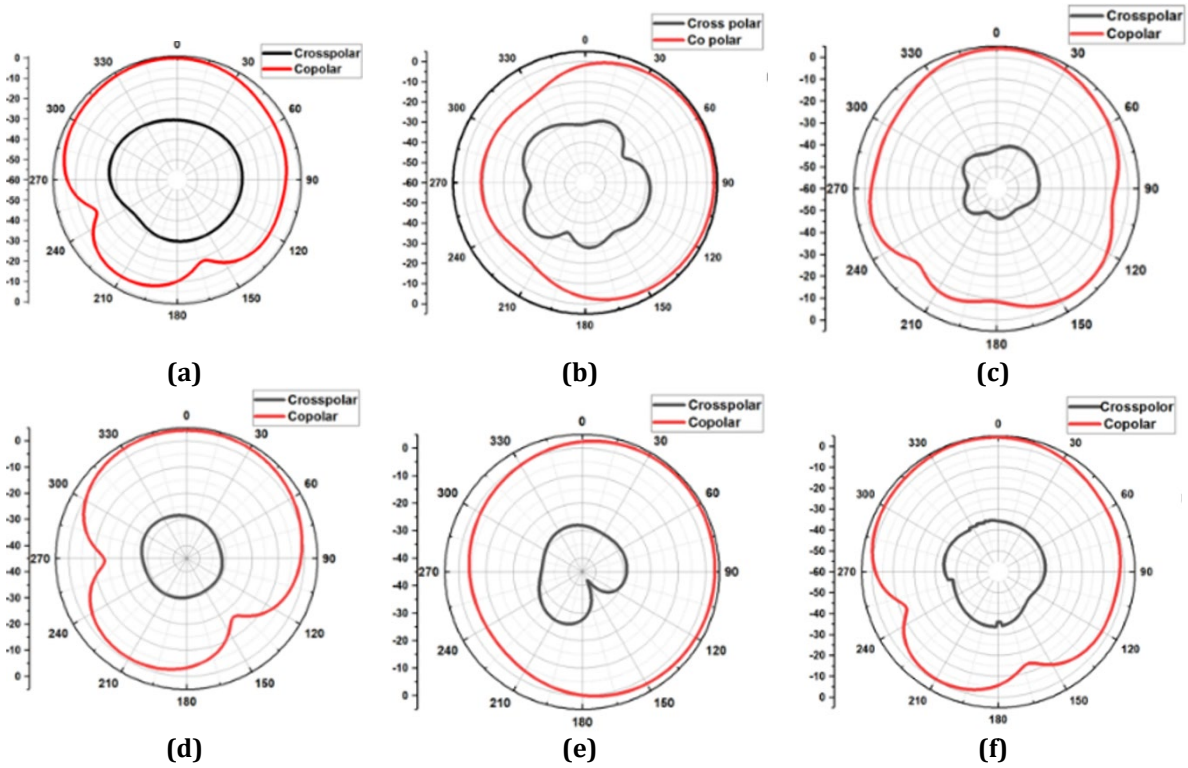

Fig. 8 *Simulated 2D radiation patterns and YZ plane (a) 2THZ in XZ; (b) 5THz in XZ;(c)15THz in XZ;(d) 2THZ in YZ; (e) 5THz in YZ;(f)15THz in YZ*

3.1 Diversity Characteristics of DNG-PDGS Loaded Dual Port MIMO Antenna

To validate MIMO antenna diversity performance, the diversity parameters like Envelope Correlation Coefficient (ECC), Diversity gain (DG), Total Active Reflection Coefficient (TARC), Channel capacity, and Channel capacity loss (CCL) have been discussed in this section. The quantity of correlation for two radiators has been computed by ECC parameters in [29]. When the distribution of power is uniformly lossless through radiating antennas then the computation of ECC is done by applying S-parameter values in equation (8).

$$\mathrm{ECC} = \frac{|S_{11}^{*}\, S_{12} + S_{21}^{*}\, S_{22}|^2}{(1 - |S_{11}|^2 + |S_{21}|^2) \times (1 - |S_{22}|^2 + |S_{12}|^2)} \tag{8}$$

In an uncorrelated MIMO system, the ideally desired value for the ECC is zero. For practical MIMO systems, acceptable values are typically ≤ 0.5. As observed in Fig.9a, the simulated ECC value using S-parameters in the super wide band(SWB) is less than 0.0025 which indicates that the proposed MIMO antenna exhibits a low level of correlation between its antenna elements. Furthermore, the DG of the proposed MIMO antenna is approximately calculated using equation (9). Ideally, the diversity gain value should be close to 10dB. The simulated diversity gains of the proposed MIMO antenna, as depicted in Fig.9a, is determined to be 9.99 dB. This simulation result demonstrates the excellent diversity performance of the proposed MIMO antenna, closely approaching the desired ideal value of 10dB.

$$\mathrm{DG} = 10 \times \sqrt{1 - \mathrm{ECC}^2} \tag{9}$$

The actual performance of MIMO antenna cannot be predicted by S-parameters only. So, TARC is another parameter that is evaluated by equation (10) to predict the characteristics of designed antenna. TARC(dB) is the fraction of total replicated power to total applied power of antenna elements and gives the evidence related to S-

parameters of the proposed MIMO antenna in [29]. The TARC is simulated at different phases from 0^0 to 180^0 and all values of TARC of less than -10dB have been observed throughout the frequency range which shows the phase insensitivity of proposed antenna in Fig.9b.

$$TARC = \sqrt{\frac{(S_{ii}+S_{ij})^2 + (S_{jj}+S_{ji})^2}{2}} \tag{10}$$

Here i_{th} and j_{th} are receiving and radiating transmitting elements of proposed antenna. The channel capacity(bps/Hz) evaluates the performance of proposed M x M MIMO antenna which is the function of bandwidth and signal-to-noise ratio(SNR). Without knowing the channel conditions, power is equally feed-in transmitting radiating antennas which is mathematically expressed in equation (11).

$$C_{MXM} = k \times \left\{ log_2 \left[det \left([I] + \frac{SNR}{k} [H][H^*] \right) \right] \right\} \tag{11}$$

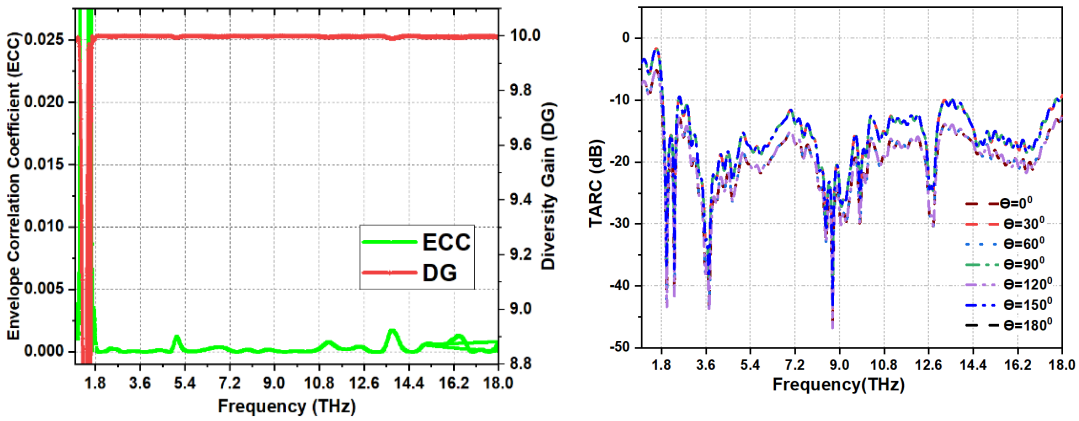

(a) **(b)**

Fig. 9 *Simulated results (a) Combine results of ECC&DG; (b) Total active reflections (TARC)*

Here k is the number of antennas for transmitting signal, fading matrix [H], and transpose of a fading matrix [H*] is Hermitian transpose of a fading matrix. identity matrix is represented by [I]. According to the authors in [29], the maximum value of channel capacity for dual port MIMO antenna is computed in equation (12), by considering the value of SNR =100 for Rayleigh fading environment. The calculated channel capacity of proposed MIMO antenna is 11.34bps/Hz which is greater than allowed channel capacity of two element MIMO antenna (7.38 bps/Hz) in [29]. The calculated and allowed limit channel capacity of proposed MIMO antenna are illustrated in Fig. 10(a).

$$C_{2-antenna\ element\ MIMO} = 2 \times log_2[1 + 50] \tag{12}$$

Moreover, channel capacity loss (CCL) defines how many numbers of bits vanished when more than two channels are utilized to transmit the signals at the time and the calculation of CCL is done by equation (13) -(16). Here φ^p is 2x2 S-correlation matrix. The ideal value should be less than 0.4 bps/Hz in [29]. As per observation in Fig. 10(b) its value is less than 0.225bps/Hz in super wide band which validates the effectiveness of the designed MIMO antenna.

$$C_{loss} = -\log_2|\varphi^p| \tag{13}$$

$$\varphi^p = \begin{bmatrix} \rho 11 & \rho 12 \\ \rho 21 & \rho 22 \end{bmatrix} \tag{14}$$

$$\rho_{ii} = 1 - \left(|S_{ii}|^2 + |S_{ij}|^2 \right) \tag{15}$$

Int. Journal of Integrated Engineering Vol. 16 No. 5 (2024) p. 311-323

$$\rho_{ij} = \left(S_{ii}^{*}S_{ij} + S_{ji}^{*}S_{ij}\right) \tag{16}$$

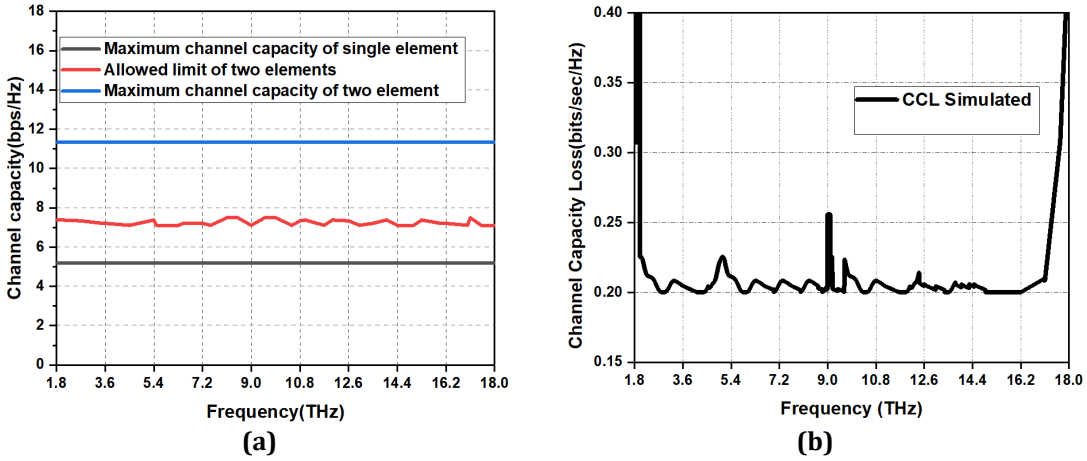

Fig. 10 *Simulated results (a) Channel capacity; (b) Channel capacity loss(CCL)*

Table 3 extracts the unique features of the proposed antenna in terms of compactness, number of radiating elements, fractional bandwidth, gain, radiation efficiency, and isolation. Diversity performance in terms of ECC and channel capacity loss is also compared with existing MIMO antennas in Table 3.

Table 3 *Assessment of reported super wideband MIMO antenna with Existing Antennas*

Ref.	S11<-10 dB Impedance Bandwidth (THz)	Gain (dBi)	η (%) **Radiation efficiency**	ECC	CCL bps/Hz	Isolation (dB) & No. of Port	Volume(μm³) & Dimensions in wavelength (λ)
[19]	1.06–14.2	11.2	NM (not measured)	<.003	0.2	<-23 (Two)	820×1000× 81.29 2.89 λ ×3.53 λ ×0.29 λ
[20]	0.3 - 15.1	NM	NM	0.02	0.2	<-13 (Two)	800×1170×81.29 0.80 λ ×1.17 λ ×0.08 λ
[22]	8.82-8.86	8.2	NM	0.0005	0.2777	<-22 (two)	35×36×5 1.03 λ×1.06 λ×0.15 λ
[23]	0.276-0.711	4	84	0.0458	0.0018	<-20 (Two)	600×300×45 0.55 λ×0.28 λ ×.041 λ
[24]	2.7-3.2	6.4	NM	NM	NM	-22 (Two)	200×220×16 1.8 λ ×1.98 λ ×.14 λ
Proposed antenna	1.75 – 18 (164%)	9.2	89	0.002	0.26	<-25 (Two)	57 ×27.6 ×3.36 0.35 λ ×0.17 λ ×.02 λ

The proposed MIMO antenna designed with two elements stands out due to its minimized profile, attributed to the small size of individual elements, distinguishing it from [19]-[20], [23]-[24]existing antennas.Moreover, DNG-PDGS loaded proposed MIMO antenna exhibits a much wider fractional bandwidth(1.75 THz to 18THz) of 164% as compared to existing antennas in[22]-[24].Unlike [24], where a vertical meta-surface placement increases overall profile and fabrication complexity, the low-profile DNG-PDGS loaded MIMO antenna enhances gain by 3dBi and reduces fabrication complexity.Furthermore, the number of elements on a larger substrate is almost same but existing antennas are having high profile and low radiation efficiency [23].Although [19],[20],[22], and [24] have not mentioned efficiency. But, the highest efficiency of proposed antenna is the more attractive parameter of the designed MIMO antenna.To endorse the good enactment for a two-element MIMO antenna, the mutual coupling between radiating elements is less than -25dB , as compared to [19]-[20],[22]-[24]. Diversity performance in terms of ECC and CCL is also compared with existing MIMO antennas in Table 3. In

summary,the proposed MIMO antenna excels in various parameters, demonstrating excellent performance for high-speed THz applications.

4. Conclusion

In this paper, a DNG-PDGS loaded MIMO antenna is designed for super wide impedance bandwidth (1.75 to 18THz) with stable omnidirectional radiation patterns for high-speed terahertz applications.By inserting double negative material-based periodic defected ground structure(DNG-PDGS) and inverse L stubs at the ground, the isolation between two radiating elements is acquired more than -25dB throughout the THz spectrum(1.75-18 THz).To validate the high-speed THz communication, a detailed evaluation is done using CST Microwave Studio by considering the diversity parameters like ECC ,DG, TARC(dB),channel capacity(bps/Hz),and channel capacity loss(bps/Hz).All compared performance parameters are listed in Table 3.Finally, the simulated results show that the SWB MIMO antenna can be a good contender for high-speed terahertz applications like in future 6G, astronomical radiometric applications.

Acknowledgement

One of authors (Ranjana Kumari) wish to express their gratitude to the management of Galgotias College of Engineering and Technology(GCET), Greater Noida for their support of this research.

Conflict of Interest

The authors declare that they have no known competing financial interests or personal relationships that could have appeared to influence the work reported in this paper. The authors have no conflict of interest to declare.

Author Contribution

*T*he authors confirm contribution to the research paper as follows: ***study conception and design of DNG-periodic defected ground structures loaded MIMO antenna for mutual coupling reduction:*** *Ranjana Kumari, V.K. Tomar;* ***Understanding of problem and finding possible solutions:*** *V.K. Tomar;* ***analysis and interpretation of results of CST microwave studio software:*** *Ranjana Kumari;* ***A rough and final draft manuscript preparation:*** *Ranjana Kumari, V.K. Tomar.* The final manuscript received the affirmation of all authors, indicating their detailed reading and approval.

References

[1] Index, C. V. N. (2015). Cisco visual networking index: Forecast and methodology 2015-2020. *White paper, CISCO*.

[2] Koenig, S., Lopez-Diaz, D., Antes, J., Boes, F., Henneberger, R., Leuther, A., & Kallfass, I. (2013). Wireless sub-THz communication system with high data rate. *Nature photonics, 7(12)*, 977-981, http://dx.doi.org/10.1038/nphoton.2013.275.

[3] Alharbi, K. H., Khalid, A., Ofiare, A., Wang, J., & Wasige, E. (2017). Diced and grounded broadband bow-tie antenna with tuning stub for resonant tunnelling diode terahertz oscillators. *IET Microwaves, Antennas & Propagation*, *11*(3), 310-316.

[4] Guo, L., Huang, F., & Tang, X. (2014). A novel integrated MEMS helix antenna for terahertz applications. *Optik, 125(1)*, 101-103.

[5] Sirmaci, Y. D., Akin, C. K., & Sabah, C. (2016). Fishnet based metamaterial loaded THz patch antenna. *Optical and Quantum Electronics*, *48*, 1-10.

[6] Mak, K. M., So, K. K., Lai, H. W., & Luk, K. M. (2017). A magnetoelectric dipole leaky-wave antenna for millimeter-wave application. *IEEE Transactions on Antennas and Propagation*, *65*(12), 6395-6402.

[7] Xue, C. D., Zhang, X. Y., Cao, Y. F., Hou, Z., & Ding, C. F. (2017). MIMO antenna using hybrid electric and magnetic coupling for isolation enhancement. *IEEE Transactions on Antennas and Propagation*, *65*(10), 5162-5170.

[8] Zhang, S., Ying, Z., Xiong, J., & He, S. (2009). Ultrawideband MIMO/diversity antennas with a tree-like structure to enhance wideband isolation. *IEEE Antennas and Wireless Propagation Letters*, *8*, 1279-1282.

[9] Liu, Y., Yang, X., Jia, Y., & Guo, Y. J. (2019). A low correlation and mutual coupling MIMO antenna. *IEEE Access*, *7*, 127384-127392.

[10] Ghoname, R., & Zekry, A. (2015). Design of a planar MIMO antenna for LTE-advanced. *International Journal of Computer Applications*, *975*, 8887.

[11] Ren, J., Hu, W., Yin, Y., & Fan, R. (2014). Compact printed MIMO antenna for UWB applications. *IEEE antennas and wireless propagation letters*, *13*, 1517-1520.

[12] Wei, K., Li, J. Y., Wang, L., Xing, Z. J., & Xu, R. (2016). Mutual coupling reduction by novel fractal defected ground structure bandgap filter. *IEEE transactions on antennas and propagation*, *64*(10), 4328-4335.
[13] Farahani, H. S., Veysi, M., Kamyab, M., & Tadjalli, A. (2010). Mutual coupling reduction in patch antenna arrays using a UC-EBG superstrate. *IEEE antennas and wireless propagation letters*, *9*, 57-59.
[14] Lee, J. Y., Kim, S. H., & Jang, J. H. (2015). Reduction of mutual coupling in planar multiple antenna by using 1-D EBG and SRR structures. *IEEE Transactions on Antennas and Propagation*, *63*(9), 4194-4198.
[15] Hafezifard, R., Naser-Moghadasi, M., Mohassel, J. R., & Sadeghzadeh, R. A. (2015). Mutual coupling reduction for two closely spaced meander line antennas using metamaterial substrate. *IEEE Antennas and wireless propagation letters*, *15*, 40-43.
[16] Ramachandran, A., Pushpakaran, S. V., Pezholil, M., & Kesavath, V. (2015). A four-port MIMO antenna using concentric square-ring patches loaded with CSRR for high isolation. *IEEE Antennas and Wireless Propagation Letters*, *15*, 1196-1199.
[17] Zhang, S., & Pedersen, G. F. (2015). Mutual coupling reduction for UWB MIMO antennas with a wideband neutralization line. *IEEE antennas and wireless propagation letters*, *15*, 166-169.
[18] Arun, H., Sarma, A. K., Kanagasabai, M., Velan, S., Raviteja, C., & Alsath, M. G. N. (2014). Deployment of modified serpentine structure for mutual coupling reduction in MIMO antennas. *IEEE Antennas and Wireless Propagation Letters*, *13*, 277-280.
[19] Singhal, S. (2020). CPW fed koch snowflake superwideband terahertz spatial diversity antenna. *Optik*, *206*, 164329.
[20] Singhal, S. (2020). Tetradecagonal ring shaped terahertz superwideband MIMO antenna. *Optik*, *208*, 164066.
[21] Saxena, G., Awasthi, Y. K., & Jain, P. (2020). High isolation and high gain super-wideband (0.33-10 THz) MIMO antenna for THz applications. *Optik*, *223*, 165335.
[22] Rubani, Q., Gupta, S. H., & Rajawat, A. (2020). A compact MIMO antenna for WBAN operating at Terahertz frequency. *Optik*, *207*, 164447.
[23] Vasu Babu, K., Das, S., Varshney, G., Sree, G. N. J., & Madhav, B. T. P. (2022). A micro-scaled graphene-based tree-shaped wideband printed MIMO antenna for terahertz applications. *Journal of Computational Electronics*, *21*(1), 289-303.
[24] Smari, B., Labidi, M., & choubani, F. (2019). Mutual coupling reduction in metamaterial antenna for terahertz application. *Applied Physics A*, *125*, 1-7.
[25] He, X. J., Qiu, L., Wang, Y., Geng, Z. X., Wang, J. M., & Gui, T. L. (2011). A compact thin-film sensor based on nested split-ring-resonator (SRR) metamaterials for microwave applications. *Journal of Infrared, Millimeter, and Terahertz Waves*, *32*, 902-913.
[26] Pan, B. C., Tang, W. X., Qi, M. Q., Ma, H. F., Tao, Z., & Cui, T. J. (2016). Reduction of the spatially mutual coupling between dual-polarized patch antennas using coupled metamaterial slabs. *Scientific reports*, *6*(1), 30288.
[27] Tung, N. T., Lam, V. D., Park, J. W., Cho, M. H., Rhee, J. Y., Jang, W. H., & Lee, Y. P. (2009). Single-and double-negative refractive indices of combined metamaterial structure. *Journal of Applied Physics*, *106*(5).
[28] Smith, D. R., Schultz, S., Markoš, P., & Soukoulis, C. M. (2002). Determination of effective permittivity and permeability of metamaterials from reflection and transmission coefficients. *Physical review B*, *65*(19), 195104.
[29] Saxena, G., Jain, P., & Awasthi, Y. K. (2020). High diversity gain super-wideband single band-notch MIMO antenna for multiple wireless applications. *IET Microwaves, Antennas & Propagation*, *14*(1), 109-119.